PHILOSOPHICAL TRANSACTIONS OF THE ROYAL SOCIETY A MATHEMATICAL, PHYSICAL & ENGINEERING SCIENCES

Unsteady separated flows over manoeuvring lifting surfaces

George N. Barakos and Dimitris Drikakis

Phil. Trans. R. Soc. Lond. A 2000 **358**, 3279-3291
doi: 10.1098/rsta.2000.0708

10.1098/rsta.2000.0708

THE ROYAL SOCIETY

Unsteady separated flows over manoeuvring lifting surfaces

By George N. Barakos† and Dimitris Drikakis‡

University of Manchester Institute of Science and Technology, Department of Mechanical Engineering, PO Box 88, Manchester M60 1QD, UK

Numerical simulations of dynamic-stall phenomena have been performed using an implicit unfactored Navier–Stokes solver and various turbulence closures, including linear and nonlinear low-*Re* eddy-viscosity models. The accuracy of the models has been assessed against a range of experimental data for ramping and oscillating aerofoils at subsonic and transonic conditions. The computations indicate that the nonlinear eddy-viscosity models better predict the shedding of the dynamic-stall vortex and the unsteady aerodynamic loads.

Keywords: dynamic stall; unsteady aerodynamic flows; pitching aerofoils

1. Introduction

The numerical simulation of unsteady turbulent flows around moving solid bodies is motivated by the industrial need to analyse and understand flow phenomena associated with the behaviour of aircraft during manoeuvres. The complex flow phenomena and interactions that occur during super-manoeuvrable, high-incidence flight are highly nonlinear due to massive separation and interactions between vortices, solid bodies, turbulent boundary layers, and shock waves. Subsequently, the numerical simulation of the above phenomena poses many challenges with respect to numerical methods and turbulence models.

The present paper focuses on the phenomenon of *dynamic stall* (DS) arising from unsteady pitching of aerofoils. The DS process has been under investigation for over three decades and significant progress has been made towards understanding the physical interactions associated with rapidly manoeuvring lifting surfaces beyond the static stall angle. Reviews of past theoretical and experimental works can be found in the papers of Telionis (1977), McCroskey *et al*. (1982) and McCroskey (1981), while another experimental study was more recently published by Piziali (1993). Past computational studies by Mehta & Lavan (1975), Tuncer (1988), Carr (1988), Visbal (1988) and Ekaterinaris (1995) have analysed the DS phenomenon in laminar and turbulent flow conditions. All the aforementioned computational studies have indicated that the accuracy of numerical calculations is strongly affected by the realism of the turbulence model. Experience with algebraic turbulence models has

† Present address: Department of Engineering, Imperial College of Science, Technology and Medicine, London SW7 2AZ, UK.

‡ Present address: Department of Engineering, Queen Mary, University of London, London E1 4NS, UK.

shown that such approximations do not provide satisfactory results in most cases. Linear low-*Re* two-equation models seem to offer a reasonable balance between accuracy and computational cost, but are not able to capture important effects arising from normal-stress anisotropy.

At present, nonlinear eddy-viscosity models (NLEVMs) (see, for example, Suga 1995; Craft *et al*. 1996) emerge as an intermediary level in the hierarchy of closure models incorporating key features of second-moment closure, but with a computational effort similar to that for simple isotropic eddy-viscosity two-equation models. The key idea behind NLEVMs can be found in the work of Pope (1975) and Speziale (1987), while Rubinstein & Barton (1990) have also developed NLEVMs based on renormalization group theory. Suga (1995) and Craft *et al*. (1996) developed two- and three-equation low-*Re* NLEVMs, and their studies indicate that these models are able to give results close to those obtained by second-moment closure. Their models employ a cubic expansion of the Reynolds-stress tensor in terms of the strain and vorticity invariants, in contrast to the quadratic expansion proposed by Speziale (1987).

In addition to turbulence modelling, another challenging task in the simulation of unsteady aerodynamic flows is the development of accurate and efficient numerical methods for the unsteady solution of the Navier–Stokes and turbulence-transport equations. In the past, many researchers have developed Navier–Stokes methods for unsteady inviscid and viscous flows based on explicit schemes, implicit approximate-factorization schemes, or hybrid schemes (Visbal 1988; Ekaterinaris 1995). Explicit schemes require the use of very small time-steps, which lead, subsequently, to long computing times. Approximate-factorization schemes allow larger time-steps but still place tight constraints on the maximum Courant–Friedrichs–Lewy (CFL) number, especially in three-dimensional flows. On the other hand, implicit unfactored schemes which use Newton sub-iterations allow high CFL numbers and are less sensitive to the choice of time-step than approximate-factorization schemes.

In the present work, an implicit unfactored solver developed by Barakos & Drikakis (1998, 1999) has been used for the coupled solution of the Navier–Stokes and turbulence model equations. Validation has been undertaken for various aerodynamic flows including quasi-steady flows over aerofoils and unsteady flows over oscillating and ramping aerofoils.

2. Mathematical modelling

(*a*) *Governing equations*

The governing equations are the two-dimensional, Reynolds-averaged, compressible Navier–Stokes equations in conservation-law form. Additional equations are required to model turbulence transport. It should be noted that the use of averaged equations to model unsteady flows is only justified if the unsteadiness due to the imposed boundary conditions is not modulating the inherent unsteadiness due to turbulence.

The governing equations are employed in conservation-law form for an inertial frame of reference (IFR) (x_0, z_0, t). However, to numerically simulate flows around moving bodies, a non-inertial frame of reference (NIFR) needs to be considered (figure 1). The relative velocity of the NIFR with respect to the IFR is

$$\boldsymbol{V} = \boldsymbol{V}_0(t) + \boldsymbol{\Omega}(t)(\boldsymbol{r}(t) - \boldsymbol{r}_0(t)). \tag{2.1}$$

PHILOSOPHICAL TRANSACTIONS OF THE ROYAL SOCIETY A MATHEMATICAL, PHYSICAL & ENGINEERING SCIENCES

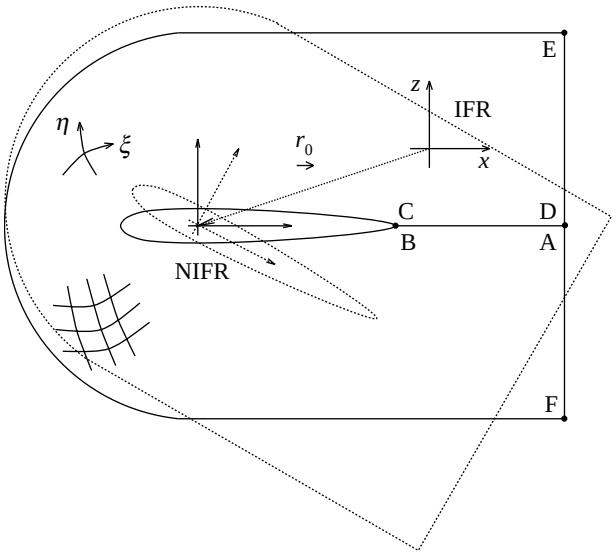

Figure 1. Schematic of the flow domain.

For a pure rotation of the frame of reference, $\boldsymbol{V}_0(t)$ vanishes. Further simplifications can be obtained by placing the origin of the NIFR at the origin of the IFR ($\boldsymbol{r}_0(t) = \boldsymbol{0}$). Finally, for two-dimensional problems and rotation of the NIFR about a single axis, $\boldsymbol{\Omega}(t)$ becomes a scalar, ω_f.

The prescribed pitching motion can, subsequently, be used to find the parameter $\omega_\mathrm{f} = \mathrm{d}\alpha/\mathrm{d}t$. For all test cases presented in this work the aerofoil is subjected to a harmonic oscillation about its quarter-chord axis (figure 1), which is described in terms of the angle-of-incidence variation, $\alpha(t)$, using

$$\alpha(t) = \alpha_0 + \alpha_1 \cos(\omega_\mathrm{f} t), \tag{2.2}$$

where α_0 and α_1 are the mean angle and amplitude of the harmonic oscillation, respectively. In the case of oscillating aerofoils, the unsteady motion is usually characterized by the similarity parameter k_f, known as reduced frequency of the oscillation. This is defined by

$$k_\mathrm{f} = \omega_\mathrm{f} c/2U_\infty, \tag{2.3}$$

where c is the characteristic length of the problem (aerofoil chord), ω_f is the frequency of the oscillation, and U_∞ is the freestream velocity.

(*b*) *Turbulence modelling*

The stress tensor $t_{ij} = \bar{t}_{ij} + \tau_{ij}^\mathrm{R}$ contains molecular and Reynolds-stress contributions. Linear eddy-viscosity models of the k–ϵ type require the solution of two transport equations, one for the kinetic energy of turbulence, k, and one for the turbulent dissipation rate, ϵ (or its isotropic component $\tilde{\epsilon}$). These models make use of the Boussinesq approximation to model the Reynolds stress tensor. On the other hand, NLEVMs use an expansion of the Reynolds-stress components in terms of the mean strain-rate and rotation tensors:

$$S_{ij} = \tfrac{1}{2}(U_{i,j} + U_{j,i}), \qquad \Omega_{ij} = \tfrac{1}{2}(U_{i,j} - U_{j,i}). \tag{2.4}$$

In view of the marginal improvements returned, generally, by quadratic expansions, a cubic expansion has been proposed by Suga (1995) and employed in this work. For the k–ϵ NLEVM of Suga (1995), the transport equations for k and $\tilde{\epsilon}$ are similar to those of the standard k–ϵ model of Launder & Sharma (1974). The production term P_k suggested by Suga (1995) is:

$$P_k = \rho c_\mu f_\mu \tilde{\epsilon} \tilde{S} \tilde{\Omega}. \tag{2.5}$$

Also the coefficient c_μ in the calculation of the eddy viscosity ($\mu_{\mathrm{T}} = c_\mu \rho f_\mu (k^2/\tilde{\epsilon})$) is not a constant any more, but is given by a function that involves the strain and vorticity invariants. Such a functional form of c_μ has been found to be beneficial in flows far from equilibrium, and has also been employed in the work of Liou & Shih (1996) for shock–boundary layer interaction.

Apart from the cubic k–ϵ NLEVM of Suga (1995) and Craft *et al.* (1996), the linear k–ϵ models of Launder & Sharma (1974) and Fan *et al.* (1993) have also been employed in the present study. Moreover, results have also been obtained using the one-equation model of Spalart & Allmaras (1992).

(*c*) *Numerical scheme*

The present numerical scheme solves the conservation equations of mass, momentum and energy along with the turbulence-transport equations using a finite-volume approach and body-conforming curvilinear coordinates (ξ, ζ, τ).

The discretization of the inviscid fluxes is obtained by a characteristic-based scheme (approximate Riemann solver). Since this scheme has been extensively used in the past for studying steady compressible flows (Eberle *et al.* 1992; Drikakis & Durst 1994*a*, *b*), it will not be presented here in detail. A third-order upwind scheme is also used in conjunction with the Riemann solver in order to increase, locally, the accuracy of the calculation of the inviscid fluxes at the cell faces of the computational volumes (Drikakis & Durst 1994*a*, *b*). Limiters based on the square of pressure derivatives have been used for detecting shocks and contact discontinuities. The viscous terms are discretized by central differences.

The time accuracy can be obtained by using implicit or explicit schemes, and the efficiency of the above is strongly related to the time-scales imposed by the prescribed motion of the solid boundaries. The present approach solves all equations in a strongly coupled manner using an implicit unfactored relaxation scheme. This results in a compact numerical implementation that requires a moderate number of Newton iterations at each time-step. However, the implementation is complicated and also requires a realistic initial guess (e.g. the steady-state solution around a fixed boundary) before the time marching is initiated (Barakos & Drikakis 1999).

For the implicit solution of the governing equations, a second-order approximation of the time derivative has been used. For every cell of the computational domain, a diagonally dominant system of six equations can be obtained and subsequently inverted by a matrix-inversion technique. This system is solved here by a point-by-point Gauss–Seidel scheme. Moreover, to obtain high values of the CFL number, preconditioning is also performed at each Gauss–Seidel sub-iteration (Barakos & Drikakis 1998).

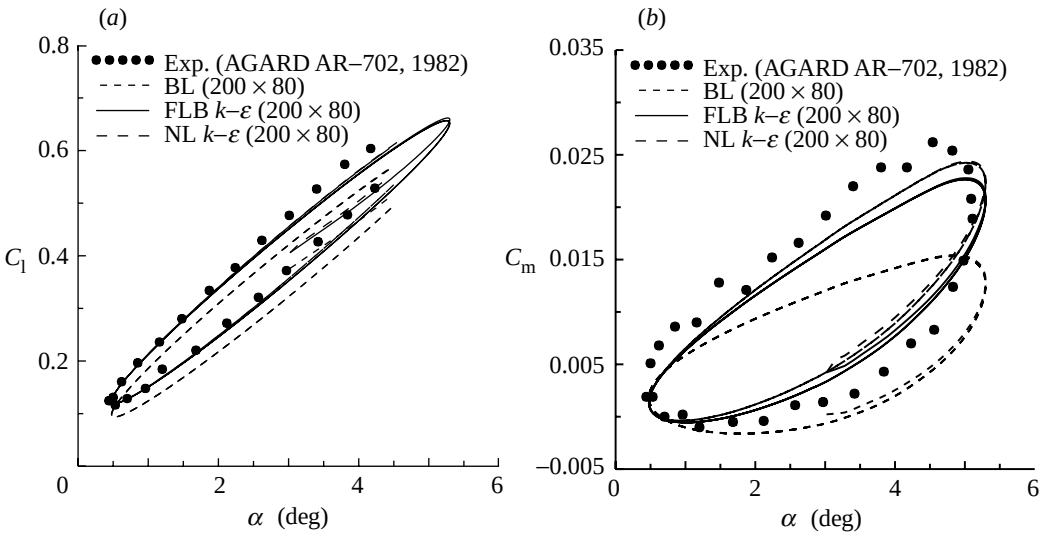

Figure 2. Unsteady airloads for the AGARD CT1 case.

3. Results and discussion

The model's performance is examined here for the NACA-0015 and NACA-0012 aerofoils. The selection of the above geometries was based on the availability of experimental data or previous simulation results from the literature.

Body-fitted, structured C-type computational grids have been used in all calculations. The grids have been generated using an elliptic grid generator. The grid lines are clustered near the body surface in the normal direction and are stretched towards the leading and trailing edge of the profile. Extra care has been taken to place enough grid points very close to the solid boundary. For all cases, the first node above the solid boundary was at a distance of $10^{-6}c$, giving $y^+ < 1$. The far-field boundary was placed at $6c$ in the upstream direction and at $10c$ in the wake direction. The grid contains 200 cells on the profile surface, 50 cells on each side of the artificial boundary in the wake, and 90 cells in the vertical direction. Thus, the total number of grid cells is 300×90. A coarser mesh (180×80) has been employed for the one-equation Spalart–Allmaras model.

The orientation of the NIFR with respect to the IFR is changing in time, and the nodal coordinates are, therefore, recomputed at each time-step. Since the grid is not deformed, the Jacobians of the cells, as well as the distance between the cells and the solid boundary, are held constant.

The boundary conditions are updated explicitly at each time-step. For all cases considered here the incoming stream is subsonic; thus, density and velocity components are held constant and the pressure is extrapolated from inside the domain. The level of the freestream turbulence has been kept constant at 0.5% of the kinetic energy of the incoming stream. A length-scale of $0.01c$ has been used to estimate the freestream value of the turbulence energy dissipation rate. At the outflow boundary, a simple extrapolation has been used for all variables. As initial conditions, the steady-state solution of the flow around the aerofoil has been used.

(a) *Harmonic oscillation of the NACA-0012–AGARD CT-1 case*

This is an unsteady transonic flow case with Mach and Reynolds numbers of 0.6 and 4.8×10^6, respectively. The mean incidence angle is 2.8° and the amplitude of oscillation is 2.4°. The aerofoil is pitched with respect to the quarter-chord axis ($x/c = 0.25$). The case is identified as CT1 in the Advisory Group for Aerospace Research and Development (AGARD) compendium of unsteady aerodynamic measurements (AGARD 1982). The linear EVM model by Fan *et al*. (1993) (hereafter referred to as FLB), as well as the algebraic Baldwin–Lomax model and the NLEVM, have been employed for this case. The lift and moment loops are shown in figure 2. Due to the high value of the freestream Mach number, a shock appears in the leading-edge region of the profile. The relative strength of the shock changes as the aerofoil oscillates. Due to the small incidence angles the flow is essentially attached, and, thus, sensitivity to turbulence modelling is expected to be modest. However, the moment loop shows significant differences between numerical predictions and experimental data.

(b) *Deep-stall oscillation of the NACA-0015*

Experiments for the unsteady flow over an oscillating NACA-0015 aerofoil have been performed by Piziali (1993) and these are used herein. The experimental results include hysteresis loops of the lift, drag and moment coefficients. The leading-edge transition was fixed using trips attached to the aerofoil surface. The data correspond to deep-stall conditions at which the static stall angle is exceeded. Deep-stall flows are encountered in helicopter rotors and such cases are especially challenging, both for the flow solver and turbulence models.

In order to carry out the unsteady computations, the quasi-steady turbulent flow over the aerofoil at mean angle was computed first and this solution was given as the initial condition to initiate the unsteady flow computation. The freestream conditions correspond to a Reynolds number of 1.95×10^6 and a Mach number of 0.29. The amplitude of the oscillation is 4.2°, while the mean incidence is 17°. For all cases the reduced frequency of the oscillation is $k_\mathrm{f} = 0.1$. Numerical results for the above case have also been presented by Ekaterinaris (1995) using an implicit factorization method. The Spalart–Allmaras (SA), the Launder–Sharma (LS) and the NLEVM k–ϵ model (NL) were employed in the present computations. Quasi-steady computations indicated that separation occurs at 13° for all models. Therefore, only unsteady solutions should be carried out for higher incidence angles.

Results for unsteady airload hysteresis loops are shown in figure 3. The calculations performed with the NLEVM are in better agreement with the experimental data. For the same regime, the linear LS model gives poor results due, mainly, to the excessive production of turbulence it predicts. The NLEVM, and to some extent the SA model, predicts lower levels of turbulence and, thus, the DS vortex separates more readily. The results for the C_l coefficient (figure 3) show that the predictions of the two models are comparable for some parts of the unsteady cycle, except at high angles of incidence, where the NLEVM predictions are closer to the experimental data. Such differences are more pronounced in the C_m loop. Finally, it is observed that the trends of the moment coefficient are better predicted by the two-equation models, but the differences between computations and experiment remain large.

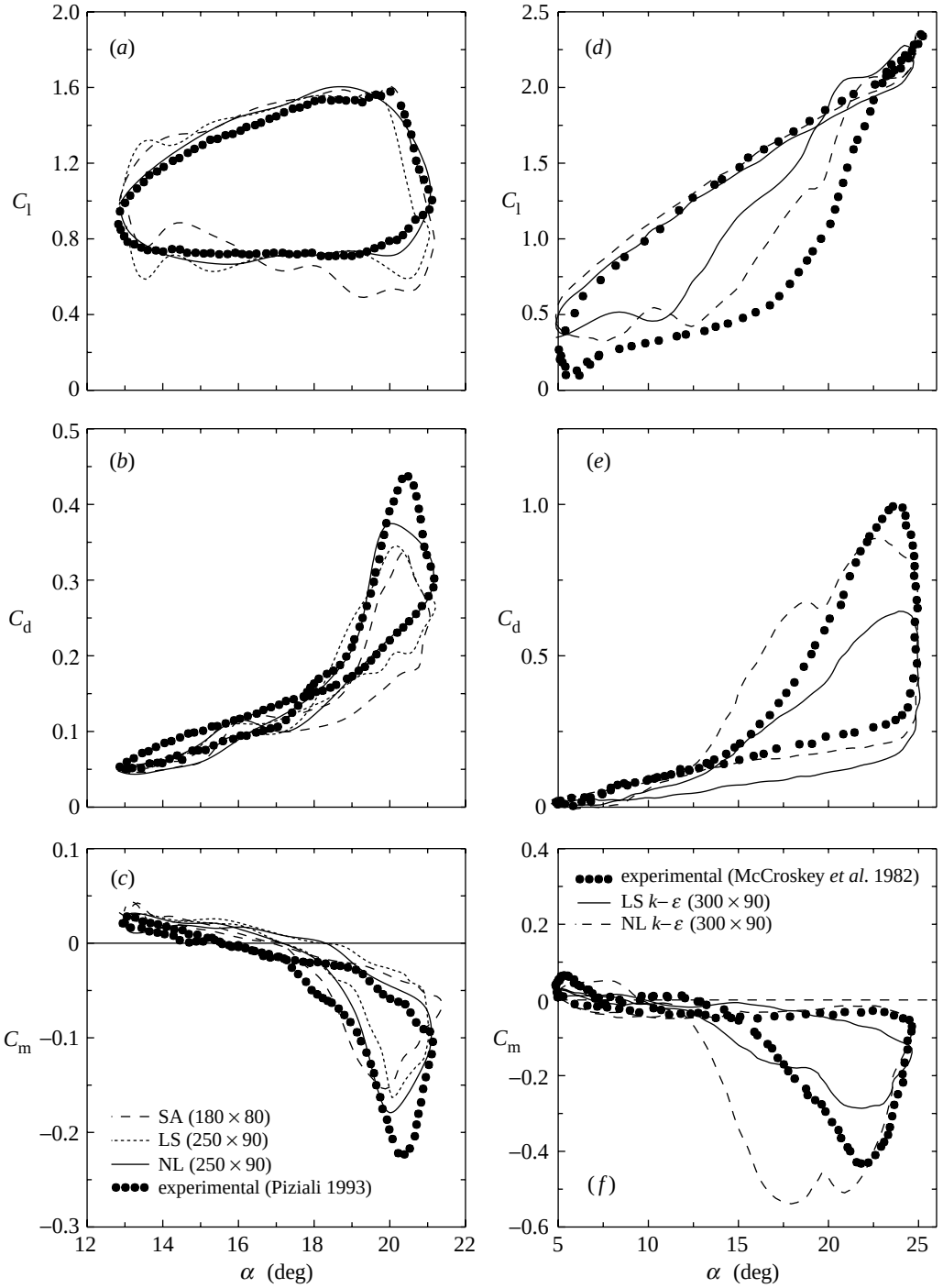

Figure 3. Unsteady airloads for the oscillating NACA-0015 ((*a*)–(*c*)) and oscillating NACA-0012 ((*d*)–(*f*)) aerofoils.

(c) *Deep-stall oscillation of the NACA-0012*

Computations at deep-stall conditions have also been performed for the NACA-0012 profile. The results are compared with the experimental data of McCroskey (1981). The freestream Reynolds-number is 10^6, while the Mach number is 0.2. The oscillation amplitude is 10° around a mean incidence angle of 15° and the reduced frequency is $k_f = 0.25$. The LS and NLEVM models were employed for this flow case.

As can be seen from the predicted unsteady airloads (figure 3*d–f*), the linear model fails to predict essential features of the loop curves. In particular, the 'double loop' of the C_m (figure 3*e*) is suppressed. This is apparently due to the excessive production of turbulence, which inhibits flow separation and results in poor predictions of the lift and moment loops. A better prediction has been obtained by the NLEVM.

(d) *Ramping NACA-0012*

The flow simulation around a ramping NACA-0012 aerofoil was also carried out. Ramping is a common case for investigating the unsteady aerodynamics of a lifting surface, and, therefore, several experimental investigations have been performed in the past (AGARD 1982; Wilby 1996; Mabey *et al*. 1988). In the present work, the Mach and Reynolds numbers are 0.56 and 4.5×10^6, respectively, while a dimensionless pitch rate of 0.85 deg s^{-1}, non-dimensionalized by U_∞/c, is used. The starting incidence is 0° and varies up to the maximum of 15°. This case was selected since it combines relatively high Mach number and stall occurring at high incidence angles. Figure 4 shows the C_l coefficient predicted by linear and nonlinear EVM in comparison with experimental results reported in AGARD (1982). Comparisons between simulation results and experimental data at three time instants are also shown in the same figure. At low incidence angles the flow is attached and both linear and nonlinear EVMs satisfactorily predict the experimental values. At higher incidence angle, and as a shock is formed close to the leading edge of the aerofoil, there is some improvement using the NLEVM. However, there is still a significant discrepancy between the predictions and experimental data. After stall and as the aerofoil reaches the maximum incidence, the predictions of the models are similar with large differences between their predictions and experimental data, especially close to the leading edge of the profile (see figure 4*d*).

(e) *Discussion*

A summary of the results obtained so far, as well as an overview of the phenomena predicted by the calculations, is given below. Figure 5 presents the time history of the aerodynamic loads using the NLEVM. Figure 5*a* suggests that for the CT1 case (moderate Mach number, small mean and oscillation amplitude angles) there is a smooth variation of the C_p coefficient during the unsteady oscillation, resulting in a simple hysteresis loop. Moving to higher incidence angles (NACA-0015 and NACA-0012 cases) the phenomenon of dynamic stall takes place. Figure 5*b* presents the surface pressure history for the NACA-0012 aerofoil oscillating at deep-stall subsonic conditions. It is evident that there is an abrupt change of the C_p coefficient as the maximum incidence is reached. The shedding of the dynamic stall vortex (DSV) is evident in figure 5*b*, indicated by a second peak in the C_p curve. The DSV travels over the profile and is then shed in the wake (three last C_p curves in figure 5*b*). The

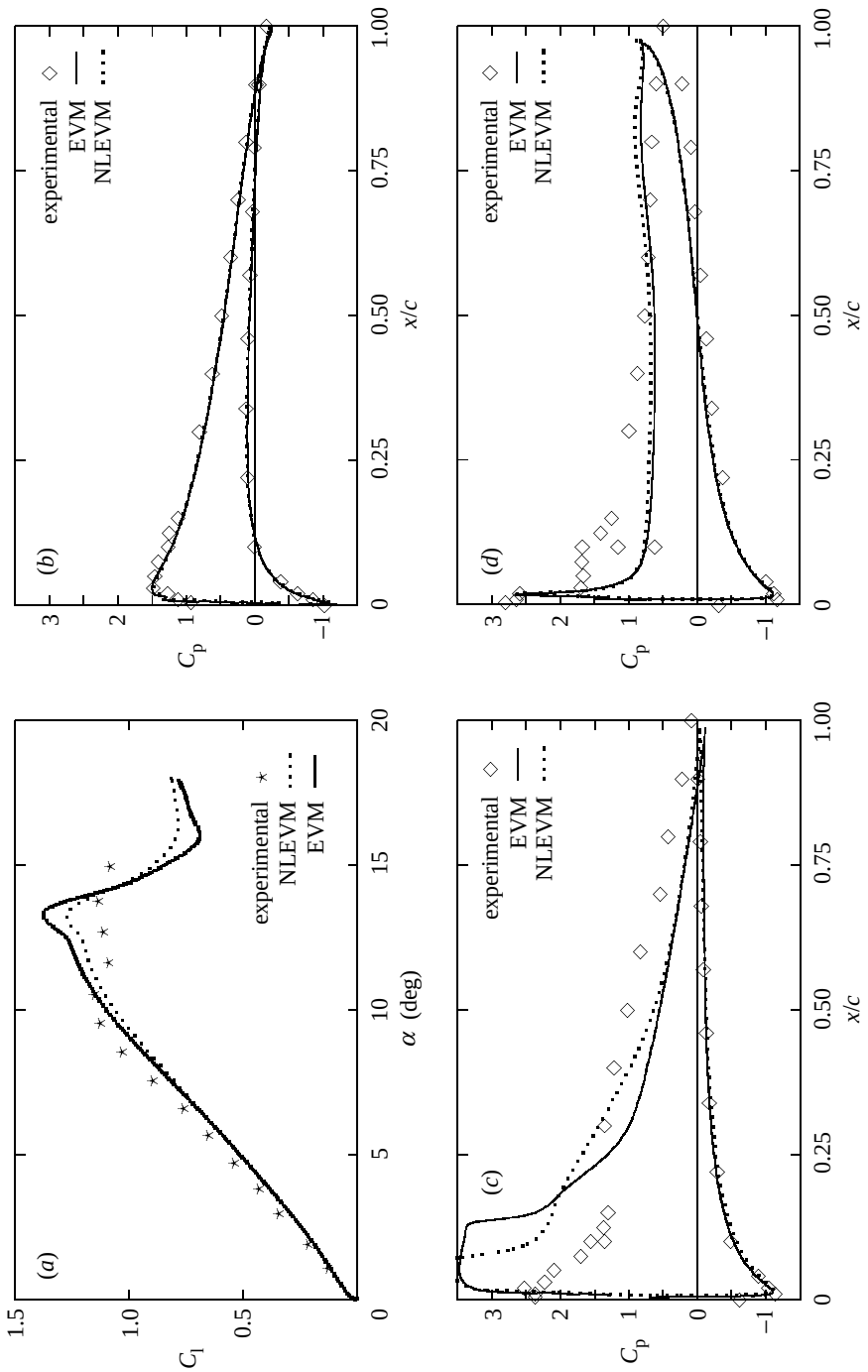

Figure 4. Ramping NACA-0012 aerofoil. (*a*) Lift curve. Comparison between numerical and experimental results for the C_p coefficient at (*b*) 5°, (*c*) 10.5° and (*d*) 15°.

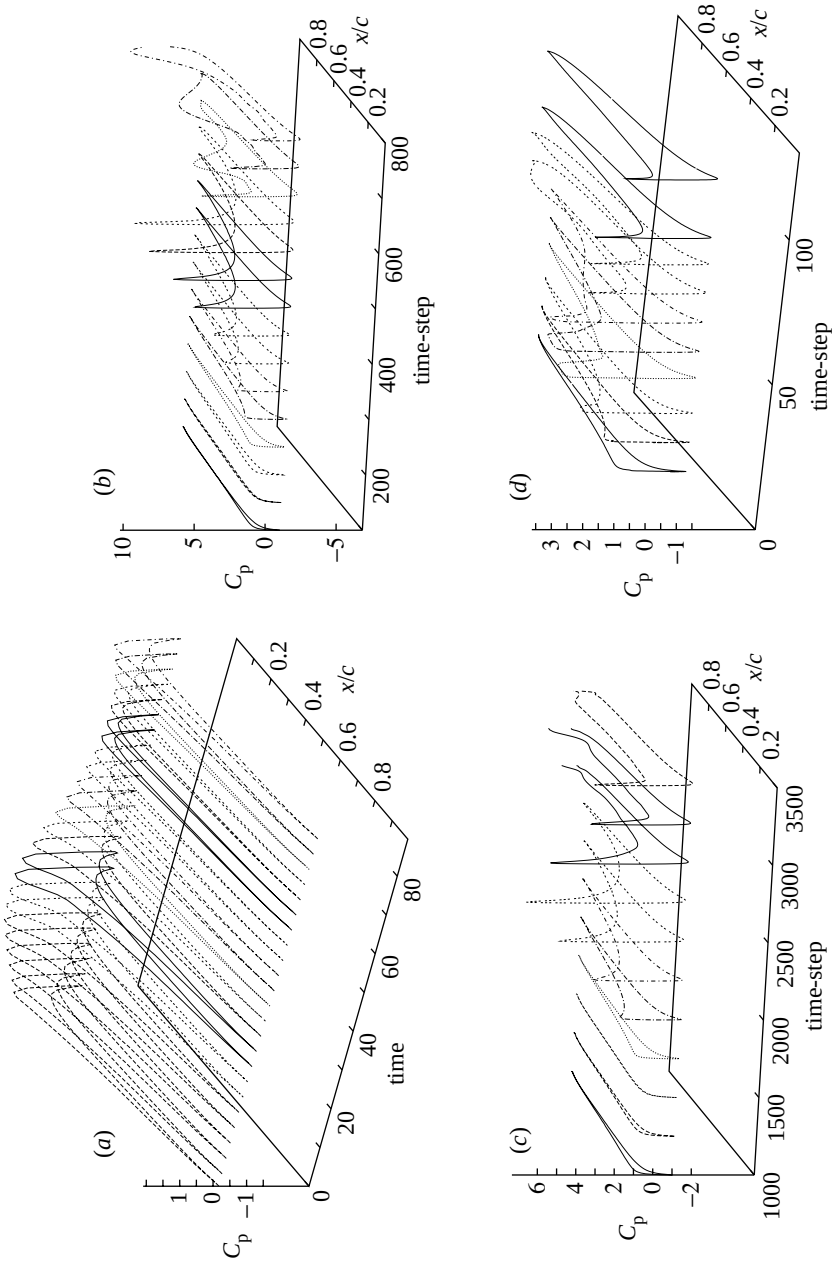

Figure 5. Surface pressure history (*a*) for the AGARD CT-1 case, (*b*) for the oscillating NACA-0012 at deep-stall conditions, (*c*) for the oscillating NACA-0012 at low frequency, and (*d*) for the ramping NACA-0012. All time-steps correspond to results before and after the stall angle.

combination of maximum incidence and pitch rate can lead to either a single loop of the C_m coefficient (NACA-0015 case) or a double-loop (NACA-0012) case. This phenomenon is totally different from the static stall of an aerofoil, where separation

initially occurs at the trailing edge and the stall angle is smaller. Figure 5*c* shows the history of the C_p coefficient for an oscillating NACA-0012 at low frequency. The conditions are close to those of the deep-stall oscillating NACA-0012 aerofoil, but the reduced frequency of oscillation is much smaller ($k_f = 0.05$). As shown, the DSV is not present and vortex shedding occurs directly at the trailing edge as the stall angle is approached. This is essentially a quasi-steady calculation—pitching at very low rate—and the stall angle is the same with the static one. For a higher Mach number—the case of ramping NACA-0012—the separation of the boundary layer appears to be associated both with the moving boundary and with the shock–boundary-layer interaction. Figure 5*d* shows the time history of the C_p for the case of the ramping NACA-0012. The presence of a shock is evident in the middle of the plot, at dimensionless time-step equal to about 50, while vortex shedding occurs earlier. The path of the vortex around the profile is not as clear as for the subsonic case, since separation starts downstream of the shock.

The CPU time for a single time-step, as well as the number of time-steps needed for every period of oscillation, depend strongly on the flow case and turbulence model employed. For all unsteady cases examined in this paper, calculations were performed for three full oscillation loops to assure that periodic loads have been obtained. The number of time-steps per oscillation cycle varied from 48 for the CT1 case to 145 for the deep-stall oscillation of the NACA-0012. The CPU time per step doubles when a two-equation model is employed instead of an algebraic one. The NLEVM was found to be more difficult to converge and required a further reduction of the CFL number. For the most difficult case considered here (oscillating NACA-0012 at deep-stall conditions), three days of CPU time were required to obtain results using the NLEVM model. The computations were performed on a single processor of the SGI ORIGIN-2000.

4. Conclusions

An implicit unfactored solver for the coupled solution of the Navier–Stokes and turbulence-transport equations was employed to calculate unsteady aerodynamic flows with moving boundaries. The results demonstrated that the numerical predictions depend strongly on the turbulence closure employed. The NLEVM model was found to predict better results than the linear EVM and captured many features that appeared in the experimental data.

Using the present numerical scheme in conjunction with the employed turbulence models we were able to reproduce qualitatively well-known phenomena associated with the unsteady flow, such as the DSV, DS, the leading edge and trailing edge separation, the hysteresis of the airloads, and the unsteady shock–boundary-layer interaction. Further progress is, however, necessary in terms of the accuracy of the turbulence models in order to obtain better results compared with the experimental data. Moreover, further improvements of the efficiency of CFD solvers is required when these are used in conjunction with complex turbulence closures.

Various parts of this work were supported by the EPSRC/MoD (GR/L18457) in collaboration with GKN Westland Helicopters and by the Brite/EuRam project UNSI.

The UNSI project (Unsteady Viscous Flow in the Context of Fluid–Structure Interaction) is a collaboration between Alenia, BAe, CASA, Dasa-M (Coordinator), Dassault, DERA, DLR, FFA, IMFT, IRPHE, NUMECA, ONERA, Saab, TUB and UMIST/QMW. The project is funded by

PHILOSOPHICAL TRANSACTIONS OF THE ROYAL SOCIETY A MATHEMATICAL, PHYSICAL & ENGINEERING SCIENCES

the European Union and administrated by the CEC, DG XII, Brite/EuRam, IMT (project ref. BRPR-CT97-0583).

References

AGARD 1982 Compendium of unsteady aerodynamic measurements. Advisory report no. 702.

Barakos, G. & Drikakis, D. 1998 Implicit-unfactored implementation of two-equation turbulence models in compressible Navier–Stokes methods. *Int. J. Numer. Meth. Fluids* **28**, 73–94.

Barakos, G. & Drikakis, D. 1999 An implicit unfactored method for unsteady turbulent compressible flows with moving boundaries. *Comp. Fluids* **28**, 899–921.

Carr, L. W. 1988 Progress in analysis and prediction of dynamic stall. *J. Aircraft* **25**, 6–17.

Craft, T. J., Launder, B. E. & Suga, K. 1996 Development and application of a cubic eddy-viscosity model of turbulence. *Int. J. Heat Fluid Flow* **17**, 108–115.

Drikakis, D. & Durst, F. 1994*a* Investigation of flux formulae in transonic shock wave/turbulent boundary layer interaction. *Int. J. Numer. Meth. Fluids* **18**, 385–413.

Drikakis, D. & Durst, F. 1994*b* A numerical study of viscous supersonic flow past a flat plate at large angles of incidence. *Phys. Fluids* **6**, 1553–1573.

Eberle, A., Rizzi, A. & Hirschel, E. H. 1992 *Numerical solutions of the Euler equations for steady flow problems*. Notes on Numerical Fluid Mechanics, vol. 34. Wiesbaden: Vieweg.

Ekaterinaris, J. A. 1995 Numerical investigation of dynamic stall of an oscillating wing. *AIAA J.* **33**, 1803–1808.

Fan, S., Lakshminarayana, B. & Barnett, M. 1993 Low-Reynolds-number k–ϵ model for unsteady turbulent boundary-layer flows. *J. AIAA* **31**, 1777–1784.

Launder, B. E. & Sharma, B. I. 1974 Application of the energy-dissipation model of turbulence to the calculation of flow near a spinning disk. *Lett. Heat Mass Transfer* **1**, 131–138.

Liou, W. W. & Shih, T. H. 1996 Transonic turbulent flow predictions with two-equation turbulence models. NASA contractors' report no. 198444, ICOMP-96-02. Lewis, OH: NASA.

Mabey, D. G., Welsh, B. L. & Pyne, C. R. 1988. A summary of measurements of steady and oscillatory pressures on a rectangular wing. *Aero. J.* **92**, 10–28.

McCroskey, W. J. 1981 The phenomenon of dynamic stall. NASA technical memorandum no. 81264. Ames, CA: NASA.

McCroskey, W. J., McAlister, K. W., Carr, L. W. & Pucci, S. L. 1982 An experimental study of dynamic stall on advanced airfoil sections, vol. 1. Summary of the experiment. NASA Technical Memorandum no. 84245. Ames, CA: NASA.

Mehta, U. B. & Lavan, Z. 1975 Starting vortex, separation bubbles and stall: a numerical study of laminar unsteady flow around an airfoil. *J. Fluid Mech.* **67**, 227–256.

Piziali, R. A. 1993 An experimental investigation of 2D and 3D oscillating wing aerodynamics for a range of angle of attack including stall. NASA technical memorandum no. 4632. Ames, CA: NASA.

Pope, S. B. 1975 A more general effective-viscosity hypothesis. *J. Fluid Mech.* **72**, 331–340.

Rubinstein, R. & Barton, J. M. 1990 Nonlinear Reynolds stress models and the renormalization group. *Phys. Fluids* A **2**, 1472–1476.

Spalart, P. R. & Allmaras, S. R. 1992 A one-equation turbulence model for aerodynamic flows. AIAA paper 92-0439.

Speziale, C. G. 1987 On nonlinear K–l and K–ϵ models of turbulence. *J. Fluid Mech.* **178**, 459–475.

Suga, K. 1995 Development and application of a non-linear eddy viscosity model sensitized to stress and strain invariants. PhD thesis, University of Manchester Institute of Science and Technology, UK.

Telionis, D. P. 1977 Unsteady boundary layers, separated and attached. AGARD CP-227, Unsteady Aerodynamics, paper 16.

Tuncer, I. H. 1988 Unsteady aerodynamics of oscillating and rapidly pitched airfoils. PhD thesis, Georgia Institute of Technology, Atlanta, GA, USA.

Visbal, M. R. 1988 Effect of compressibility on dynamic stall. AIAA Paper 88-0132.

Wilby, P. G. 1996 The development of rotor aerofoil testing in the UK. The creation of a capability to exploit a design opportunity. *Proc. 1996 European Rotorcraft Forum*, pp. 18-1–18-11.

PHILOSOPHICAL TRANSACTIONS OF THE ROYAL SOCIETY A MATHEMATICAL, PHYSICAL & ENGINEERING SCIENCES

PHILOSOPHICAL TRANSACTIONS OF THE ROYAL SOCIETY A MATHEMATICAL, PHYSICAL & ENGINEERING SCIENCES
PHILOSOPHICAL TRANSACTIONS OF THE ROYAL SOCIETY A MATHEMATICAL, PHYSICAL & ENGINEERING SCIENCES